GUST LOAD ALLEVIATION ON A LARGE BLENDED WING BODY AIRLINER

Andreas Wildschek*, Felix Stroscher, Thomas Klimmek***, Zbyněk Šika****, Tomáš Vampola****, Michael Valášek****, Dagfinn Gangsaas*****, Nicky Aversa******, Adrien Berard******

*EADS Innovation Works, **Technische Universität München, ***Deutsches Zentrum für Luft- und Raumfahrt, ****Czech Technical University in Prague, *****DG Aviation, ******AIRBUS France

e-mail: andreas.wildschek@eads.net

Keywords: *Blended Wing Body Airliner, Gust Load Alleviation, Gust Load Analysis*

Abstract

This paper investigates the gust load response of a large 750 passenger Blended Wing Body (BWB) airliner for identification of sizing cases for the aircraft structure. Considering manoeuvre load alleviation, gust loads become the dominant sizing factor for the BWB airplane. In order to allow for structural weight saving a Gust Load Alleviation System (GLAS) is designed and evaluated by numeric simulations.

1 Introduction

For a significant fuel efficiency improvement on long-range transport aircraft, the transition to Blended Wing Body (BWB) configurations offers a promising long term solution. The advantage of higher lift to drag ratio is opposed by technical challenges such as the design of a flat pressurized cabin, specific demands on the control system due to the high coupling between flap deflections and aircraft movements in all three axes, or handling asymmetric engine failure as discussed in WILDSCHEK ET AL. [1].

Moreover, due to the low wing loading BWB aircraft are generally more sensitive to vertical gust (in comparison to manoeuvre loads) than conventional wing tube aircraft. The research on aircraft consisting only of a wing dates back to the 1930s, when the German Horten Brothers built their first flying wing airplanes [2]. In LIEBECK [3] some of the problems listed above are discussed based on a design of a BWB subsonic civil transport aircraft, however handling gust loads is not mentioned.

HILEMAN ET AL. [4] show environmental advantages of the BWB configuration such as lower noise signature with buried engines. Buried engines would also ease the problem of handling asymmetric engine failure without a tail. The strategic B-2 bomber, the only flying wing aircraft in service today, combines efficient aerodynamics for long range transport with a low radar cross section. As explained in BRITT ET AL. [5] this aircraft requires a quite sophisticated control system in order to handle gust loads. The weight penalty imposed by the B2's large high bandwidth control surfaces including structural reinforcement in order to be able to transmit the high actuator forces however are impractical for a civil BWB airliner where the main focus is on fuel efficiency.

Chapter 2 describes the generation of a parameterized state space model of the coupled flight dynamic-aeroelastic equations of motion of a BWB airliner. The order of this model is subsequently reduced for control law design and validation by a combination of objective methods (balanced reduction) and prior choice of preserved states (i.e. all flight mechanics states, lag states).

In Chapter 3 the design of the basic flight controls is illustrated. A gust load alleviation system (GLAS) for the large 750 passenger BWB airliner is applied for structural weight saving. In order to estimate the gust load reduction achieved by the GLAS numeric simulation results are outlined in Chapter 4.

2 Aircraft Model

The aircraft model used for loads analysis and design and validation of the GLAS is based on aerodynamic and structural data of the BWB configuration NACRE-FW1 developed in the European project NACRE [6]. Figure 1

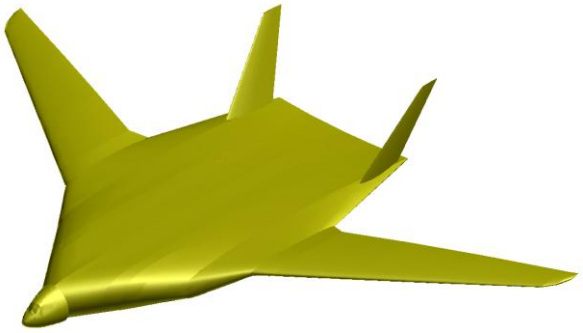

Fig. 1. Geometry without engines of the NACRE-FW1 configuration

illustrates the geometry of the NACRE-FW1.
The original model of the primary structure of the NACRE-FW1 configuration was not designed for dynamic analysis. Necessary modifications and extensions were required which comprise integration of additional structural elements for improved stiffness. Components like cockpit, elevators, rudders, wings' leading and trailing edges, landing gears, as well as engine and pylon structure were replaced by concentrated masses, see Figure 2.

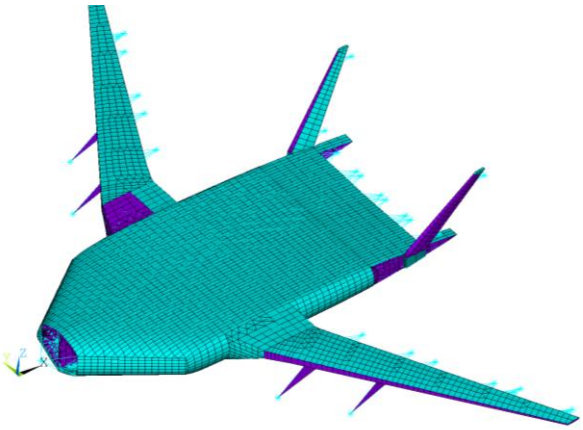

Fig. 2. Modified and extended finite element model of the NACRE-FW1 configuration

Non-structural masses of systems and equipment as well as operational masses (as defined in the NACRE project) were integrated into the structural model. Finally, various passenger/payload and fuel configurations were modelled with concentrated masses and also integrated into the structural model of the NACRE-FW1 configuration, see Figure 3. Such prepared sets of structural models were reduced to the first 100 structural Eigen modes [7].

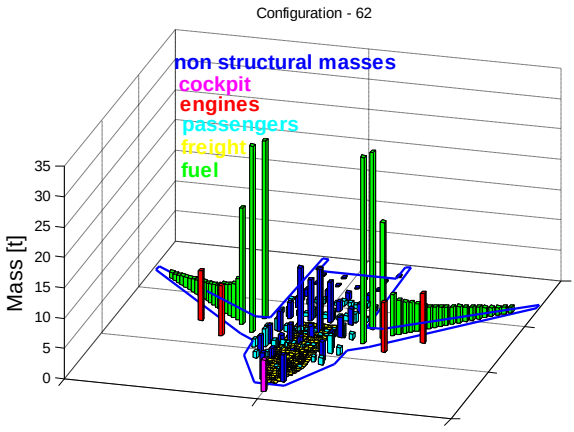

Fig. 3. Scheme of non-structural masses

2.1 Model Parameterization

The four parameters considered in the model are altitude and Mach number as well as fuel filling level and passenger/payload mass. For the fuel filling 7 variants ranging from empty to full are considered whereas for passenger/payload 3 variants (i.e. 0% – dashed lines, 50% – dotted lines, and 100% – solid lines) are considered. The acronyms for the 21 passenger/payload and fuel configurations are illustrated in Table 1. Labelled line styles are used in all subsequent figures in chapter 3 and in chapter 4.

Table 1. Mass variants

	passenger/payload		
Fuel – line colour	0%	50%	100%
0 – black lines	00	01	02
1/16 – blue lines	10	11	12
1/8 – green lines	20	21	22
¼ – red lines	30	31	32
½ – cyan lines	40	41	42
¾ – magenta lines	50	51	52
1 – yellow lines	60	61	62

Fuel mass configurations are set up in order to stay within the centre of gravity (CG) range defined in the NACRE project. Figure 4 illustrates the mass and CG variations for the 21 mass variants.

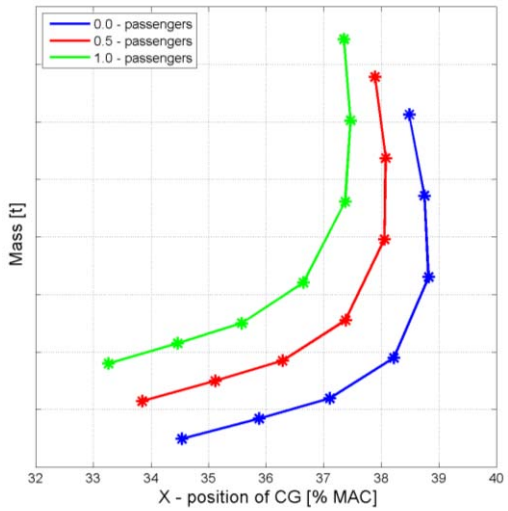

Fig. 4. Mass and CG variations for the 21 mass variants

For the parametrization of flight conditions 11 Mach numbers are considered ranging from Ma = 0.2 to Ma = 0.88. For each Mach number 8 different flight levels are defined, see Figure 5.

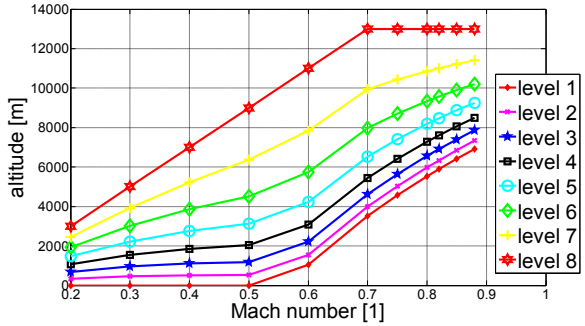

Fig. 5. Points for altitude and Mach number parameterization

2.2 Computation of Static Wing Loads

For the computation of structural loads at 1g level flight the aircraft finite element model is loaded by gravitational forces as well as aerodynamic forces that were computed by trim analysis for 1g level flight.

Using the estimated loads, cut forces and moments were evaluated at the wing root, see Figure 6.

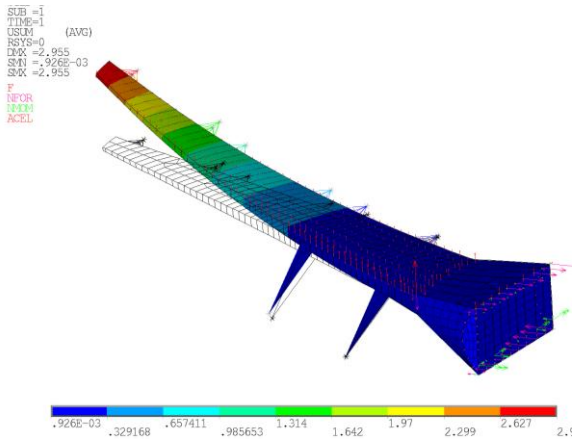

Fig. 6. Deformation of the wing due to gravitational and aerodynamic forces at 1g level flight, Ma = 0.85, q = 11069Pa

2.3 Steady Aerodynamics

Aerodynamic polars, damping derivatives, and control surface derivatives were provided by the NACRE project for various low and high speed cases. The used analysis methods range from surface panel methods to CFD. The control surfaces of the investigated BWB airliner are illustrated in Figure 7.

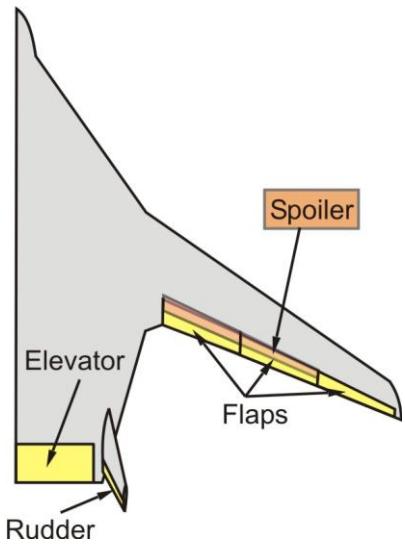

Fig. 7. BWB control surface setting

2.4 Unsteady Aerodynamics

Mass-normalised mode shapes $\mathbf{\Phi}$ of the unconstrained structure are computed by modal decomposition. Unsteady aerodynamic forces are projected to this set of degrees of freedom (DOF). Rigid body modes, which will later account for aerodynamic forces in flight dynamics, are normalized to displacements of 1m for translational modes, respectively 1rad for rotational modes. The Aerodynamic Influence Coefficient matrix $\mathbf{A}_{IC}$ is computed by the subsonic panel method ZONA6, within the Aeroelastic Toolkit ZAERO [8]. Matrix $\mathbf{A}_{IC}$ relates normal wash $\mathbf{w}$ to unsteady pressure coefficients $\mathbf{C}_\mathbf{p}$ on aerodynamic panels, which are normalized by dynamic pressure. Matrices $\mathbf{A}_{IC}(ik)$ are computed in frequency domain for a set of reduced frequencies k.

$$\mathbf{C}_\mathbf{p} = \left[\mathbf{A}_{IC}(ik)\right]^T \mathbf{w} \tag{1}$$

$$\text{with } k = \frac{\omega c}{2V_\infty} \tag{2}$$

Thereby, ω is the angular frequency, c is the reference chord length and V_∞ denotes the free stream velocity. By the use of an integration matrix $\mathbf{S}_{KJ}$, $\mathbf{C}_\mathbf{p}$ is converted to aerodynamic force coefficients in the 6 DOF directions of each panel. For the transformation of 6 DOF displacements on panels to normal wash the transformation matrix $\mathbf{F}_{JKS}$ is employed. As panel control points do not coincide with structural grid points, a spline matrix $\mathbf{G}$ is used which transforms displacements or forces from structural to aerodynamic DOF. Finally, the modal matrix $\mathbf{\Phi}$, on structural DOF, transforms the aerodynamic force coefficients to modal coordinates resulting in the Generalized Aerodynamic Forces (GAF) due to modal deflection $\mathbf{Q}_{hh}$. GAF due to control surface deflection $\mathbf{Q}_{hc}$ and due to gust downwash $\mathbf{Q}_{hg}$ are computed by right-hand side multiplication with control surface modes $\mathbf{\Phi}_c$ and gust modes $\mathbf{\Phi}_g$ [8], see Eq. (3).

$$\begin{aligned}
\mathbf{Q}_{hh}(ik) &= \mathbf{\Phi}^T\mathbf{G}^T\left[\mathbf{S}_{KJ}\right]^T\left[\mathbf{A}_{IC}(ik)\right]^T\left[\mathbf{F}_{JKS}(ik)\right]^T\mathbf{G}\,\mathbf{\Phi} \\
\mathbf{Q}_{hc}(ik) &= \mathbf{\Phi}^T\mathbf{G}^T\left[\mathbf{S}_{KJ}\right]^T\left[\mathbf{A}_{IC}(ik)\right]^T\left[\mathbf{F}_{JKS}(ik)\right]^T\mathbf{G}\,\mathbf{\Phi}_c \\
\mathbf{Q}_{hg}(ik) &= \mathbf{\Phi}^T\mathbf{G}^T\left[\mathbf{S}_{KJ}\right]^T\left[\mathbf{A}_{IC}(ik)\right]^T\left[\mathbf{F}_{JKS}(ik)\right]^T\mathbf{G}\,\mathbf{\Phi}_g
\end{aligned} \tag{3}$$

In order to derive equations of motion in time-domain, the GAF are approximated in Laplace-domain by the Minimum-State Method [9]. By replacing $i\omega$ with the Laplace variable s the approximation formula in Laplace domain writes:

$$\begin{aligned}
\mathbf{Q}_{hh}(s) &= \mathbf{A}_{hh0} + \frac{c}{2V_\infty}\mathbf{A}_{hh1}s + \left(\frac{c}{2V_\infty}\right)^2\mathbf{A}_{hh2}s^2 + \mathbf{D}\left(\mathbf{I}s - \frac{2V_\infty}{c}\mathbf{R}\right)^{-1}\mathbf{E}_h s \\
\mathbf{Q}_{hc}(s) &= \mathbf{A}_{hc0} + \frac{c}{2V_\infty}\mathbf{A}_{hc1}s + \mathbf{D}\left(\mathbf{I}s - \frac{2V_\infty}{c}\mathbf{R}\right)^{-1}\mathbf{E}_c s \\
\mathbf{Q}_{hg}(s) &= \mathbf{A}_{hg0} + \frac{c}{2V_\infty}\mathbf{A}_{hg1}s + \mathbf{D}\left(\mathbf{I}s - \frac{2V_\infty}{c}\mathbf{R}\right)^{-1}\mathbf{E}_g s
\end{aligned} \tag{4}$$

The system matrices of the aeroelastic equations of motion, $\mathbf{K}$, $\mathbf{B}$, and $\mathbf{M}$ are composed of approximation matrices of aerodynamic forces and structural portions, i.e. modal stiffness $\mathbf{K}_{\text{struct}}$, modal damping $\mathbf{B}_{\text{struct}}$ and modal mass $\mathbf{M}_{\text{struct}}$ [8].

$$\begin{aligned}
\mathbf{K} &= \mathbf{K}_{\text{struct}} + q_\infty\mathbf{A}_{hh0} \\
\mathbf{B} &= \mathbf{B}_{\text{struct}} + q_\infty\left(\frac{c}{2V_\infty}\right)\mathbf{A}_{hh1} \\
\mathbf{M} &= \mathbf{M}_{\text{struct}} + q_\infty\left(\frac{c}{2V_\infty}\right)^2\mathbf{A}_{hh2}
\end{aligned} \tag{5}$$

2.5 Coupled Equations of Motion

The aspired inputs to the coupled flight dynamic-aeroelastic model are control surface deflections, gust inputs, and engine thrust. The outputs are accelerations, rates and angular displacements at the CG, vertical accelerations of the wing tips, angle of attack and sideslip angle, as well as cut forces and moments at the wing roots and vertical stabilizer roots. The aeroelastic input equation for rigid and elastic motion in state-space form [8] reads:

$$\dot{x} = \begin{Bmatrix}\dot{\mathbf{q}}\\ \ddot{\mathbf{q}}\\ \dot{\mathbf{x}}_\mathbf{a}\end{Bmatrix} = \mathbf{A}_{ss}x + \mathbf{B}_{ss}u = \begin{bmatrix} 0 & \mathbf{I} & 0 \\ -\mathbf{M}^{-1}\mathbf{K} & -\mathbf{M}^{-1}\mathbf{B} & -q_\infty\mathbf{M}^{-1}\mathbf{D} \\ 0 & \mathbf{E}_h & \frac{V}{L}\mathbf{R} \end{bmatrix}\begin{Bmatrix}\mathbf{q}\\ \dot{\mathbf{q}}\\ \mathbf{x}_\mathbf{a}\end{Bmatrix} + \begin{bmatrix} 0 & 0 & 0 & 0 \\ -q_\infty\mathbf{M}^{-1}\mathbf{A}_{hC_0} & -\frac{q_\infty L}{V}\mathbf{M}^{-1}\mathbf{A}_{hC_1} & -\frac{q_\infty}{V}\mathbf{M}^{-1}\mathbf{A}_{hG_0} & -\frac{q_\infty L}{V^2}\mathbf{M}^{-1}\mathbf{A}_{hG_1} \\ 0 & \mathbf{E}_C & 0 & \frac{1}{V}\mathbf{E}_G \end{bmatrix}\begin{Bmatrix}\boldsymbol{\delta}\\ \dot{\boldsymbol{\delta}}\\ \boldsymbol{\eta}\\ \dot{\boldsymbol{\eta}}\end{Bmatrix} \tag{6}$$

Thereby, $\mathbf{q}$, $\mathbf{x}_\mathbf{a}$, $\boldsymbol{\delta}$, and $\boldsymbol{\eta}$ denote vectors of modal deflections, aerodynamic lag states, control surface deflections, and gust velocities.

In order to account for realistic flight dynamics, the steady aerodynamic data (see chapter 2.3) for the rigid aircraft is used to build up linear 6 DOF flight-dynamics equations of motion [10]. By similarity transformation the rigid body states, namely translations *Tx*, *Ty*, *Tz* and rotations *Rx*, *Ry*, *Rz* and their time derivatives are transformed to flight-dynamic states:

$$\mathbf{x}_{F,lon} = \begin{bmatrix} x \\ u \\ h \\ w \\ \theta \\ q \end{bmatrix} = \begin{bmatrix} -1 & 0 & 0 & 0 & 0 & 0 \\ 0 & 0 & 0 & -1 & 0 & 0 \\ 0 & 1 & 0 & 0 & 0 & 0 \\ 0 & 0 & V_\infty & 0 & -1 & 0 \\ 0 & 0 & 1 & 0 & 0 & 0 \\ 0 & 0 & 0 & 0 & 0 & 1 \end{bmatrix} \begin{bmatrix} T_x \\ T_z \\ R_y \\ \dot{T}_x \\ \dot{T}_z \\ \dot{R}_y \end{bmatrix} \qquad (7)$$

$$\mathbf{x}_{F,lat} = \begin{bmatrix} y \\ \beta \\ p \\ r \\ \phi \\ \psi \end{bmatrix} = \begin{bmatrix} 1 & 0 & 0 & 0 & 0 & 0 \\ 0 & 0 & 1 & \frac{1}{V_\infty} & 0 & 0 \\ 0 & 0 & 0 & 0 & -1 & 0 \\ 0 & 0 & 0 & 0 & 0 & -1 \\ 0 & -1 & 0 & 0 & 0 & 0 \\ 0 & 0 & -1 & 0 & 0 & 0 \end{bmatrix} \begin{bmatrix} T_y \\ R_x \\ R_z \\ \dot{T}_y \\ \dot{R}_x \\ \dot{R}_z \end{bmatrix} \qquad (8)$$

The resulting state vector $\mathbf{x}$, contains the 12 airframe states, followed by elastic mode states ξ, their first time derivatives $\dot{\xi}$ and lag states $\mathbf{x}_a$, see Eq. (9).

$$\mathbf{x} = \begin{bmatrix} \mathbf{x}_{F,lon} & \mathbf{x}_{F,lat} & \xi & \dot{\xi} & \mathbf{x}_a \end{bmatrix}^T \qquad (9)$$

The flight dynamic portion of the equations of motion, i.e. the 12x12 sub-matrix of the matrix A_{ss} related to the airframe states, has to represent the true flight dynamic behaviour of the aircraft and can now be replaced by linear flight-dynamics, derived from steady aerodynamics.

The measurement equations read:

$$\begin{Bmatrix} \mathbf{y}_F \\ \mathbf{y}_{struct} \\ \dot{\mathbf{y}}_{struct} \\ \ddot{\mathbf{y}}_{struct} \\ \mathbf{y}_{moment} \end{Bmatrix} = \begin{bmatrix} \mathbf{C}_F \\ \mathbf{C}_{def} \\ \mathbf{C}_{vel} \\ \mathbf{C}_{vel}\mathbf{A}_{ss} \\ \mathbf{C}_{moment} \end{bmatrix} x + \begin{bmatrix} 0 \\ 0 \\ 0 \\ \mathbf{C}_{vel}\mathbf{B}_{ss} \\ 0 \end{bmatrix} \begin{Bmatrix} \boldsymbol{\delta} \\ \dot{\boldsymbol{\delta}} \\ \boldsymbol{\eta} \\ \dot{\boldsymbol{\eta}} \end{Bmatrix} \qquad (10)$$

Where $\mathbf{C}_F$, $\mathbf{C}_{def}$, $\mathbf{C}_{vel}$, and $\mathbf{C}_{moment}$ are the output matrices for flight-dynamics $\mathbf{y}_F$, structural deformations $\mathbf{y}_{struct}$, structural velocities $\dot{\mathbf{y}}_{struct}$, and wing root bending moment measurement $\mathbf{y}_{moment}$. Structural acceleration outputs $\ddot{\mathbf{y}}_{struct}$ are facilitated by the time-derivative of the structural velocity output equation and replacing $\dot{\mathbf{x}}$ by the right-hand side of the input equation (6).

2.6 Model Order Reduction

The model before reduction has 210 states including 10 lag states, 12 flight mechanic states and 188 states corresponding to elastic modes, i.e. 94 elastic modes. The first attempt of the generation of the reduced order model (ROM) has been the balanced reduction [11], [12] based on the given inputs and outputs with target model dimension (e.g. 14 states, 50 states etc.). The results illustrated in Figure 8 show that such reduction can discard some important states, like first bending modes, lag states, or even flight mechanic states.

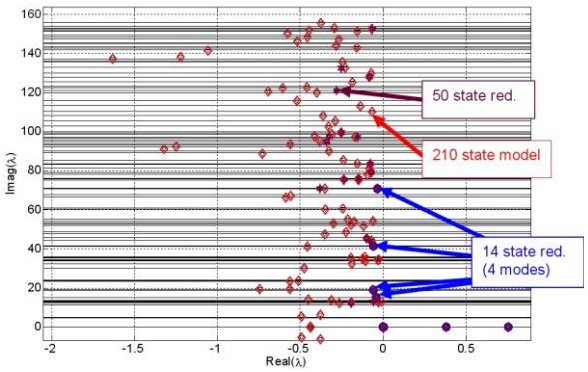

Fig. 8. Eigen values for different number of states kept in the model using balanced reduction

The red poles correspond to the initial 210 state model, magenta poles to the 50 states ROM and blue poles to the 14 states ROM. Therefore, the direct usage of the balanced reduction for all outputs and all inputs cannot be considered ideal.

Thus, a modified approach is applied. All originally included 10 lag states as well as the 12 flight mechanic states are preserved. The control law synthesis model additionally contains the first 4 (corresponding to 4 lowest Eigen frequencies) aeroelastic modes. The validation model contains 12 aeroelastic modes (i.e. modes number 1-5, 11-14, 17, 21, and 23) which were chosen using an SPA variant of balanced reduction [13].

The order reduction thereby was subsequently adapted based on the comparison of singular value characteristics and transfer functions for different levels of reduction, see Figure 9 for a comparison of transfer functions from the global vertical gust to vertical cockpit acceleration for different sets of aeroelastic modes.

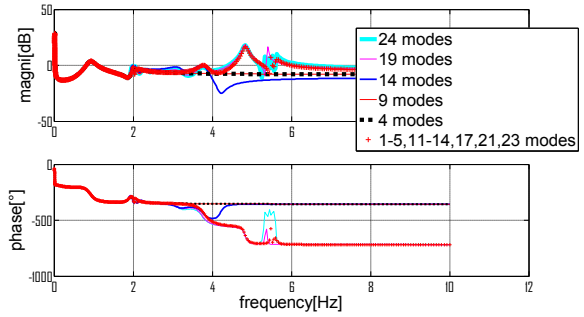

Fig. 9. Transfer functions from global vertical gust to vertical cockpit acceleration for different sets of aeroelastic modes

3 Control Design

The considered BWB airliner is statically unstable in large regions of the mass and flight envelope. Therefore, the flight control system needs to provide artificial pitch stabilization. The first wing bending mode lies at about 1 Hz and is thus difficult to separate from the angle of attack mode. The measurement signals (pitch rate, vertical acceleration at CG, etc.) are low pass filtered with a cut off frequency of about 3 Hz. Reasonable control system delays are taken into account by 2nd order Pade filters. The actuators are modelled as nonlinear subsystems taking into account that the achievable actuator deflection rate is a function of the aerodynamic forces acting on the control surface and thus a function of the deflection angle.

3.1 Flight Control Laws Design

Artificial pitch stiffness is achieved by feedback of the vertical CG load factor n_z to the elevators. In order to achieve neutral pitch stability this feedback is done via a PI controller [14]. An additional pitch damper (i.e. feedback from pitch rate q to the elevators) allows placement of the poles of the angle of attack mode.

In order to take into account handling qualities requirements the Control Anticipation Parameter (CAP) criteria is used, which provides boundaries for damping and frequency of the angle of attack mode [15].

$$CAP = \frac{\dot{q}(t=0)}{n_z(t=\infty)} \approx \frac{\left|\omega_0^2\right|_{shortperiod}}{n_\alpha} \tag{11}$$

with:

$$n_\alpha = \frac{n_z(t=\infty)}{\alpha(t=\infty)} \approx \frac{V_\infty}{g} \cdot \frac{1}{T_\mu} \tag{12}$$

Thereby, α denotes the angle of attack, and T_μ is the numerator time constant of the elevator to pitch rate zero which strongly depends on the mass variant.

The flight control law is designed robust with regards to mass and passenger/payload variation, so that only the dynamic pressure and the Mach number need to be considered for gain scheduling. Due to the variation of T_μ the optimum for the closed loop short period frequency cannot be guaranteed for all mass variants, compare Figure 10 which illustrates the closed loop poles for the 21 mass variants for Mach 0.88, altitude 7863m.

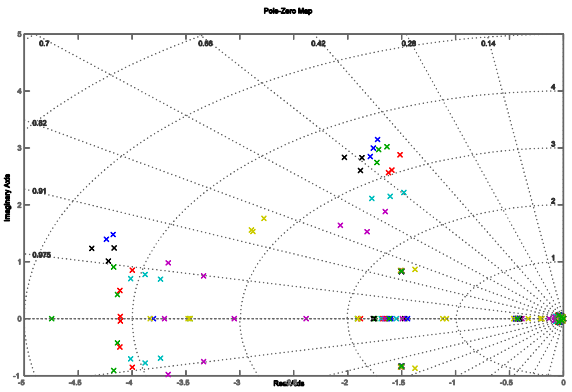

Fig. 10. Closed loop poles for 21 mass variants for Mach 0.88, altitude 7863m

The Phygoid is stabilized by PI feedback from pitch angle to elevator and by PI feedback from speed deviation to engine thrust considering a simple engine model.

3.2 Active Wing Bending Damping

Active damping of the first wing bending mode provides several advantages. Wing bending is severely excited by pitch manoeuvres. Thus, the active damping improves handling qualities. Active wing bending damping reduces wing root fatigue and reduces peak loads, mainly for downdraft gusts. Moreover, the fast spoiler deflection required for efficient gust load alleviation excites wing bending vibrations which are reduced by the active damping system. This system is based on a feedback from modal wing bending acceleration sensor Nz_{law} to symmetrically driven ailerons [16].

The requirements for the control law for active wing bending damping are a high order roll-on in order to avoid interaction with the flight control system as well as no excitation of higher flexible modes. The control law is designed robust with regards to mass and passenger/payload variation, so that only the dynamic pressure and the Mach number need to be considered for gain scheduling. The SISO control law is obtained by H_∞ synthesis using the artificially stabilized airplane as control plant. The exogenous transfer function comprises filters for roll-on, and roll-off, for uncertainty due to the different mass variants as well as for Von Kármán turbulence spectrum.

The SISO control law obtained by H_∞ synthesis has 97 states. The order is reduced to 6 states by classical tools without any significant loss of performance.

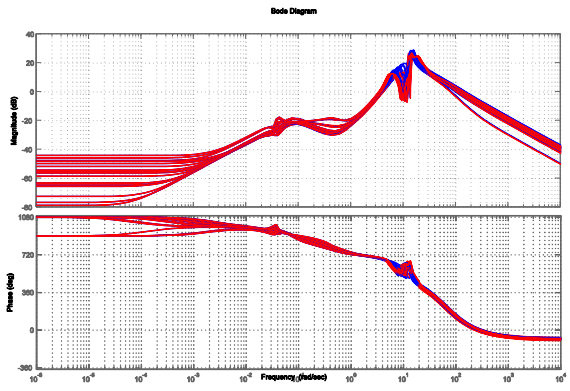

Fig. 11. Magnitudes of open loop (blue lines) and closed loop (red lines) symmetric aileron to Nz_{law} transfer functions for Mach 0.88, altitude 7863m

Figure 11 compares the magnitudes of open loop (blue lines) and closed loop (red lines) ailerons to Nz_{law} transfer functions for Mach 0.88, altitude 7863m for all mass variants except for the zero fuel case. About 5 dB reduction of the first wing bending mode peak is achieved. The Nichols plot shows a 9 dB gain margin and more than 45° phase margin, see Figure 12.

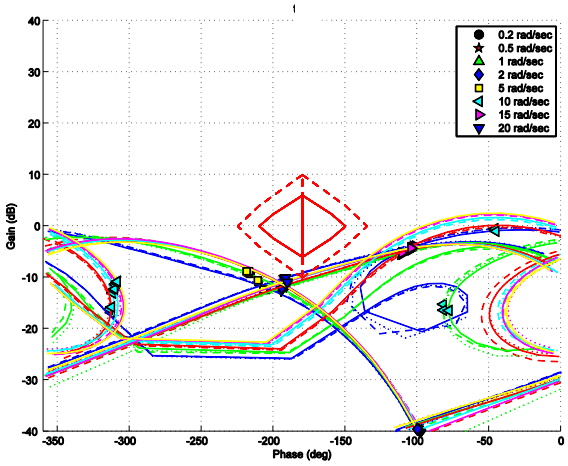

Fig. 12. Nichols plot for ailerons to Nz_{law} transfer functions for Mach 0.88, altitude 7863m for different mass variants

3.3 Dynamic Feed-Forward GLAS

As already proven in flight tests a pre-conditioned alpha probe signal is suitable as reference for dynamic feed-forward GLAS [17], [18], [19]. On the BWB airliner such a reference signal is fed through 3 dynamic filters which drive ailerons, trailing edge flaps and elevators. The commands of the dynamic feed-forward GLAS are just added to the commands of the flight control system and of the active wing bending damper. The dynamic filters minimize the cost function J:

$$J = \left\langle Nz_{law}{}^2 + \Delta C^{*2} \right\rangle \qquad (13)$$

where C^* denotes a speed dependent blending of pitch rate and n_z [14]. C^* is minimized in terms of *deviations* from pilot commands C^*_{pilot} in order to avoid unwanted compensation of pilot inputs:

$$\Delta C^* = C^* - C^*_{pilot} \qquad (14)$$

3.4 Passive GLAS using Spoilers

The passive GLAS also uses a pre-conditioned alpha probe signal. Thereby, a measurement and processing time of 40ms is considered. When the reference signal exceeds a certain threshold a spoiler deflection is commanded. The spoiler deflection command then remains constant for a pre-defined time span after which the spoilers are smoothly returned to zero position as also suggested in [16], and [20]. This open loop approach avoids parasitic feedback from the spoilers to the reference signal thus keeping the system passive. For pitch moment equilibration the elevators are commanded proportionally to the spoilers. Care needs to be taken not to induce negative load factors for reasons of safety of passengers.

4 Gust Load Reduction

Incremental wing root cut forces and moments are obtained by numeric simulation. Simulation runs are performed for manoeuvres (i.e. 2.5g pitch up, -2g pitch down) as well as for continuous turbulence and gust [21] for different mass configurations, Mach numbers and flight levels. According to the simulations vertical 1-cosine gusts with large scale lengths are sizing for the wing roots. Figure 13 illustrates the incremental wing root bending moment for updraft sizing gusts of different scale lengths as requested by the FAR [22] for the controlled aircraft without GLAS.

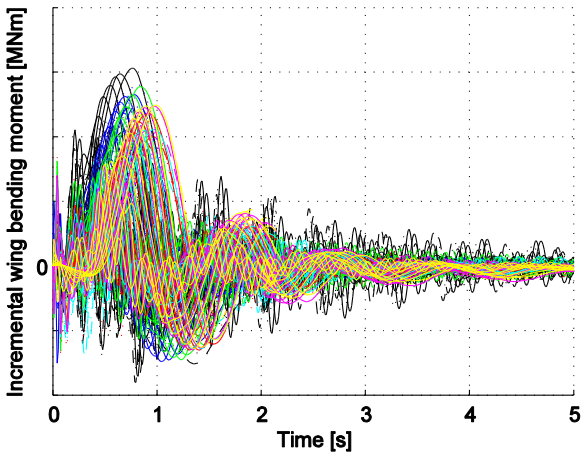

Fig. 13. Incremental wing root bending moment for updraft sizing gusts for Mach 0.88, altitude 7863m for different mass variants

The FAR does not specifically ask for scale lengths above 350 feet. Considering the sheer size of the BWB airliner however gust lengths of up to 500 feet are considered. Thereby, the most critical is found to be the 500 feet gust. Adding the 1g load the mass variant with maximum aircraft weight is the most critical for the wing root bending moment gust load.

Assuming that the gust load alleviation considerably reduces the wing bending moment in an updraft gust, other cases such as downdraft gust and manoeuvres can become sizing. Manoeuvre load alleviation is out of the scope of this paper. Downdraft gust loads are reduced by active wing bending damping as well as by dynamic feed-forward gust load alleviation. Numeric results of the incremental wing root bending moment in downdraft sizing gusts with GLAS are illustrated in Figure 14.

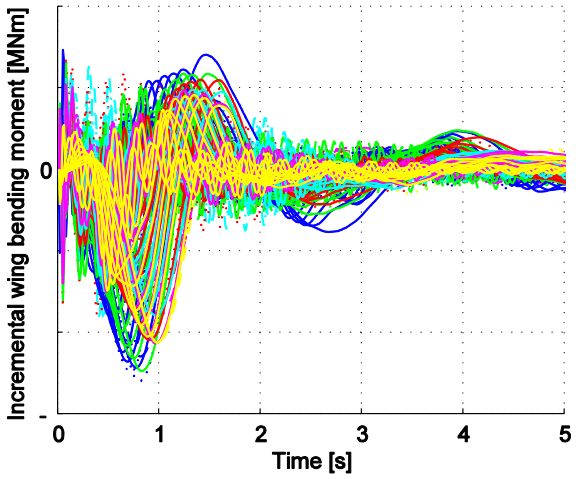

Fig. 14. Incremental wing root bending moment for downdraft sizing gusts for Mach 0.88, altitude 7863m for different mass variants with GLAS

Finally, simulation runs with GLAS were performed for updraft gusts throughout the flight envelope. In order to get an idea of how much each part of the GLAS reduces incremental wing root bending, Figure 15 shows a comparison between controlled aircraft without GLAS, with wing bending damping, with additional dynamic feed-forward gust load alleviation, and with the complete GLAS for a 500 feet sizing gust. The incremental wing bending moment is reduced by about 75%.

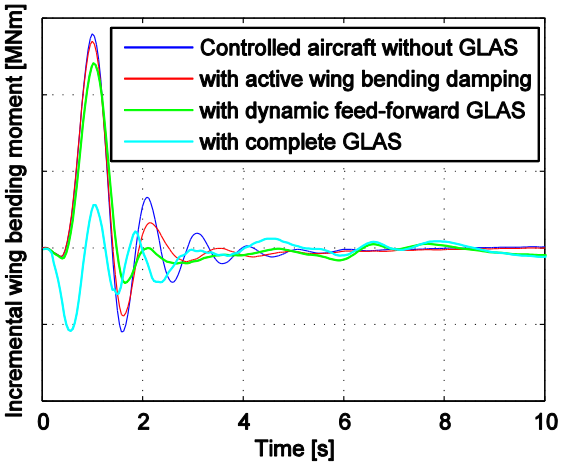

Fig. 15. Incremental wing root bending moment for a 500 feet updraft sizing gust with different controllers for maximum aircraft weight, Mach 0.88, altitude 7863m

The resulting control surface deflections are illustrated in Figure 16.

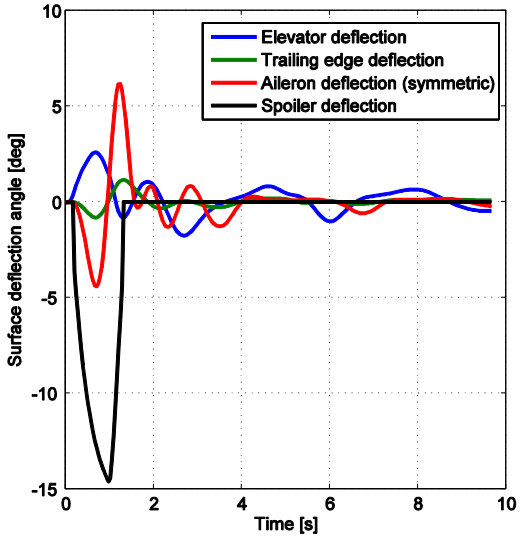

Fig. 16. Control surface deflections in a 500 feet updraft sizing gust with GLAS

For maximum total loads *with* GLAS found throughout the whole flight envelope a safety factor of 1.5 applies in order to obtain the minimum ultimate loads to be used for structural sizing. According to regulations [23], if the probability of occurrence of a GLAS failure is less than 10^{-3} per flight hour a reduced safety factor applies for the computation of ultimate loads *without* GLAS, see Figure 17.

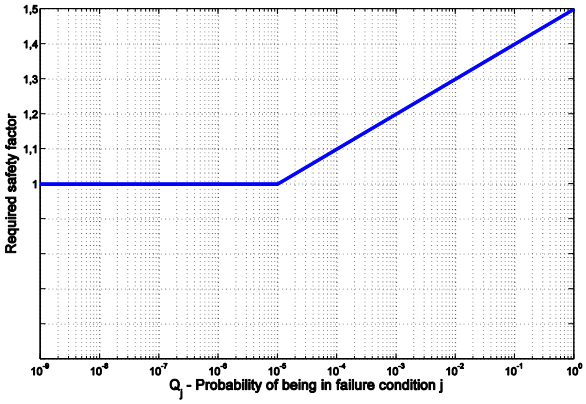

Fig. 17. Required safety factor for ultimate loads computation with GLAS in failure condition

Since the larger of these two ultimate load computations applies for structural sizing a certain reliability of the GLAS is required in order to be able to exploit the achieved gust loads reduction for structural resizing.

5. Conclusions

The gust load response of a large BWB airliner is investigated for identification of sizing cases for the structure. Design of a Gust Load Alleviation System (GLAS) is illustrated and evaluated by numeric simulations. The achieved alleviation of the wing root bending moment looks promising. Future research will be dedicated to the optimization of the open loop control of spoilers and elevators in order not to induce high negative or positive load factors by the GLAS as a trade for reduced structural loads. Structural weight saving is mainly limited by the allowed load factors considered in such optimization, by the finite control authority of the actuators, and by achievable reliability of the GLAS itself.

Acknowledgements

The authors would like to thank the European Commission for funding the ACFA2020 (Active Control for Flexible 2020 Aircraft) project within the seventh Research Framework Programme.

Many thanks also go to all ACFA2020 partners for their contributions as well as to the NACRE (New Aircraft Concepts REsearch) consortium, especially to ONERA, DLR and the NACRE-task 2.2 team, for providing aerodynamic and structure data for the flying wing aircraft.

References

[1] Wildschek A, Havar T, and Plötner K. An all-composite, all-electric, morphing trailing edge device for flight control on a blended-wing-body airliner. *Proc. IMechE, Part G: J. Aerospace Engineering*, 224(G1), pp 1-9, 2009.

[2] Myhra D. *The Horten Ho 9/Ho 229*. Schiffer Publishing Ltd., 2004.

[3] Liebeck R. Design of the Blended-Wing-Body subsonic transport. *40th AIAA Aerospace Sciences Meeting and Exhibit*, Reno, NV, Jan. 14-17, 2002.

[4] Hileman J, Spakovszky Z, Drela M and Sargeant M. Airframe design for silent aircraft. *45th AIAA Aerospace Sciences Meeting and Exhibit*, Reno, Nevada, Jan. 08-11, 2007.

[5] Britt R, Jacobson S and Arthurs T. Aero-servo-elastic Analysis of the B-2 Bomber. *Journal of Aircraft*, Vol. 37, No. 5, September/October 2000.

[6] Frota J. Novel Aircraft Concepts, *2nd NACRE Conference*, Greewich, Jul. 08-19, 2008.

[7] Valášek M, Vampola T, Šika Z, Fisch F, Baier H and Klimmek T. Adaptations on NACRE Flying Wing FEM, ACFA2020 Technical Report TR2-01, Aug. 2008.

[8] ZAERO V8.4 Users Manual.

[9] Karpel M. Design for Active Flutter Suppression and Gust Alleviation Using State-Space Aeroelastic Modelling, *Journal of Aircraft*, Vol. 19, No.3, 1982, pp 221-227.

[10] Baldelli D, Chen P, and Panza J. Unified Aeroelastic and Flight Dynamic Formulation via Rational Function Approximations. *Journal of Aircraft, Vol. 43, No. 3*, 2006.

[11] Obinata G, Anderson B. *Model reduction for control system design, communications and control engineering*. Springer, 2001.

[12] Gawronski W. *Dynamics and control of structures: a modal approach*. Mechanical Engineering Series, Springer, New York, 1998.

[13] Šika Z, Zavřel J, Valášek M. Residual modes for structure reduction and efficient coupling of substructures. *Bulletin of Applied Mechanics*, vol. 5, no. 19, pp 54-59, 2009.

[14] Brockhaus R. *Flugregelung, 2. Auflage*. Springer, Berlin, pp 655-659, 2001.

[15] Stevens B, Lewis F. *Aircraft control and simulation*. John Wiley, pp 281-291, 2003.

[16] Jeanneau M, Aversa N, Delannoy S, Hockenhull M. Awiator's study of a wing load control: design and flight-test Results, 16th IFAC Symposium on Automatic Control in Aerospace, St. Petersburg (RUSSIA), 14.-18. June, 2004.

[17] Wildschek A, Maier R, Hoffmann F, Jeanneau M, Aversa N. *Minimizing dynamic structural loads of an aircraft*. US patent US 2009/0084908, April 2009.

[18] Wildschek A, Maier R, Hahn K-U, Leißling D, Preß M, and Zach A. Flight test with an adaptive feed-forward controller for alleviation of turbulence excited wing bending vibrations. *AIAA Guidance, Navigation, and Control Conference and Exhibit*, Chicago, IL, 10.-13. August, 2009.

[19] Wildschek A, Maier R, Hromcik M, Hanis T, Schirrer A, Kozek M, Westermayer C, and Hemedi M. Hybrid controller for gust load alleviation and ride comfort improvement using direct lift control flaps. *Proc. of the 3rd European Conference for Aerospace Sciences*, Versailles, France, 2009.

[20] Fabre-Raimbault N, Adurno M, Berthereau M, Cote Stephane. *Method and device for dynamically alleviating loads generated on an airplane*. US patent US 2008/0265104, October 2008.

[21] Hoblit F. *Gust loads on aircraft: concepts and applications*. AIAA Education Series, Washington 1988.

[22] Federal Aviation Regulations, Part 25 – airworthiness standards: transport category airplanes. U.S. Department of Transportation, Federal Aviation Administration. Also: Code of Federal Regulations, title 14, aeronautics and space, Part 25 - airworthiness standards: transport category airplanes. September 1980.

[23] European Aviation Safety Agency. Certification specifications for large aeroplanes – CS25, amendment 8, 1 – App K – 2, 18 December 2009.

Copyright Statement